Radiotherapy and Oncology 134 (2019) 127–134

Contents lists available at ScienceDirect

Radiotherapy and Oncology

journal homepage: www.thegreenjournal.com

Original Article

Modeling daily changes in organ-at-risk anatomy in a cohort of pancreatic cancer patients

Alba Magallon-Baro *, Mauro Loi, Maaike T.W. Milder, Patrick V. Granton, Andras G. Zolnay, Joost J. Nuyttens, Mischa S. Hoogeman

Erasmus MC Cancer Institute, University Medical Center Rotterdam, Department of Radiotherapy, The Netherlands

ARTICLE INFO

Article history:
Received 4 September 2018
Received in revised form 10 January 2019
Accepted 22 January 2019
Available online 8 February 2019

Keywords:
Organ motion management
Daily geometric variations
Statistical motion-deformation model
PCA
SBRT
Pancreas

ABSTRACT

Purpose: To characterize daily geometrical variations of gastrointestinal organs with respect to pancreatic tumors, through a population-based statistical model.
Materials and methods: The study included 131 CT scans from 35 pancreatic cancer patients treated with Stereotactic Body Radiotherapy (SBRT). For each patient, day-to-day anatomical variations of the stomach, the duodenum and the bowel were assessed from the deformation vector fields (DVF) obtained by non-rigidly registering the contours of the fractions to the planning CT scans. For the whole population, day-to-day motion-deformation patterns were abstracted using principal component analysis (PCA) on the set of DVFs mapped on a reference patient. Based on these geometrical variations, anatomies were generated to create population-based dose-volume histograms (DVH) per patient, which were also compared to clinical values.
Results: Through PCA, the most dominant directions of daily deformations were localized in the abdominal organs. Common patterns were found, such as stomach contraction–expansion in the anterior–posterior direction ranging from 5 to 13 mm, and superior-inferior deformations on the bowel from 7 to 14 mm. The duodenum resulted to move laterally, but in a lesser extent (4–8 mm). The population-based DVHs derived from the model mostly included the daily DVHs observed in the clinic (in >90% of the cases).
Conclusions: Anatomical variations influence the delivered doses to healthy organs during SBRT. A motion model was successfully built and explored to extract the larger directions of movement of the gastrointestinal organs. Day-to-day motion modeling can potentially be used to account for geometrical uncertainties in future plan optimization and in online adaptive strategies.
 Radiotherapy and Oncology 134 (2019) 127–134

Stereotactic Body Radiotherapy (SBRT) delivers high radiation doses in a few number of fractions, making use of smaller target margins and sharp dose gradients. However, these treatment plans are traditionally based on a static snapshot of the patient anatomy, i.e. the planning CT (pCT), which in highly dynamic regions in the body, such as the pelvic or abdominal areas, leads to recurrent anatomical variations during the treatment course. For these anatomical sites, organ motion management is clearly demanded; and consequently, the challenge is to overcome these anatomical variations while maintaining target coverage and maximally sparing the surrounding healthy organs, the Organs-at-Risk (OAR).

SBRT combined with chemotherapy has emerged as a viable option for treating unresectable Locally Advanced Pancreatic Carcinomas (LAPC) [1–5]. For these patients, the proximity of the pancreas to radiosensitive gastrointestinal organs (GIO), such as the stomach, the duodenum and the bowel, limits the delivery of effective ablative radiation doses to the tumor, mainly due to the tight dose-volume constraints clinically imposed to adhere to the OAR tolerances.

At our institution, LAPC patients responding to chemotherapy receive a hypofractionated radiotherapy course of 5 × 8Gy on the CyberKnife® System using Synchrony respiratory motion tracking (Accuray Inc., Sunnyvale, CA, USA). Synchrony tracks the tumor in real-time via implanted fiducial markers, continually aligning the treatment beam by adjusting the position of the robot, which helps to ensure target coverage and OAR sparing [6,7]. However, OAR regions inevitably encounter higher doses due to day-to-day anatomic variations [8]. Until recently, these soft tissue differences could not be captured given the limitations of treatment room

* Corresponding author at: Erasmus MC Cancer Institute, University Medical Center Rotterdam, Department of Radiotherapy, Doctor Molewaterplein 40, 3015 GD Rotterdam, The Netherlands.
E-mail addresses: a.magallonbaro@erasmusmc.nl (A. Magallon-Baro), m.loi@erasmusmc.nl (M. Loi), m.milder@erasmusmc.nl (M.T.W. Milder), p.granton@erasmusmc.nl (P.V. Granton), a.zolnay@erasmusmc.nl (A.G. Zolnay), j.nuyttens@erasmusmc.nl (J.J. Nuyttens), m.hoogeman@erasmusmc.nl (M.S. Hoogeman).

https://doi.org/10.1016/j.radonc.2019.01.030
0167-8140/

imaging capabilities. However, our CyberKnife is integrated with an in-room CT-on-rails system, offering the possibility to assess moving-tissue impact nearly *in situ* [9].

Attempts to characterize OAR variations throughout the radiation course has been a topic of further interest. Deformable organ motion modeling was initially explored by Söhn et al., who suggested the use of principal component analysis (PCA) to generate a patient-specific statistical motion-deformation model of multiple organs [10]. This approach was extended by Budiarto et al., who adapted the method to allow population-based modeling, and hence, overcome the limitation of a restricted number of CT scans per subject. PCA can detect if common variation patterns are observed in a patient population even if individual organ shapes and sizes vary [11]. This method has been successfully used to understand tumor and organ motion-deformation [12–15], to evaluate margins [16,17], to simulate dosimetric treatment courses [16,18–21], to characterize respiratory-induced motion [22–24], and considered in real-time adaptive replanning for MR-guided RT [25,26]. Pelvic organs have been the main target of the above-mentioned studies, with few exceptions for head and neck [19] and thorax-lungs [14,22,23]. However, day-to-day residual motion of the abdominal organs with respect to the tumor position, as needed for improving treatments with SBRT or MR-guided RT, still remains underexplored.

The present study aims to characterize organ-at-risk daily anatomical variations and its impact in a cohort of LAPC patients. Through PCA, a statistical motion-deformation model will be derived to characterize OAR changes with respect to pancreatic tumors. Dosimetric uncertainties will be assessed by accounting for the dominant geometrical variations retrieved from the model.

Materials and methods

Patient data

Thirty-five patients with inoperable LAPC were included in this study. The data were collected retrospectively through the LAPC-1 Phase-II study (ID: NL49643.078.14), between April 2015 and November 2017. All patients underwent a combined chemoradiation treatment consisting of chemotherapy (Folfirinox) followed by a hypofractionated SBRT regime of 40 Gy in 5 fractions, prescribed to the 80% isodose line, delivered on the CyberKnife M6 system and tracked with Synchrony (Accuray Inc., Sunnyvale, CA, USA). Dose-volume constraints were set at V35Gy < 1 ml to the three critical organs, which include the stomach, the duodenum and the bowel. To ease target localization, 1 to 4 gold fiducial markers (median of 3) were implanted in a pre-treatment stage inside and/or around the pancreatic tumor. Patients were recommended to avoid solid and liquid intakes since 2 h prior to treatment.

CT images and delineations

Three to four contrast-enhanced CT scans were available per patient: one pre-treatment scan (pCT), and two or three pre-fraction in-room CT scans (FxsCT) performed under instructed end-expiration [9], using the SOMATOM Definition AS CT scanner (Siemens Healthcare, Forchheim, Germany). CT voxel size was $0.98 \times 0.98 \times 1.5$ mm^3. Eight scans were excluded for not containing the entire OAR. Overall, 131 scans were eligible for inclusion.

Delineations on the pCT were manually performed by a radiation oncologist following the RTOG guidelines of the upper abdominal region [27], including the Gross Tumor Volume (GTV) delineation. The set of OAR comprised the stomach, the duodenum and the bowel. The bowel was contoured inferiorly until L4 as a single structure, including the individual loops of the small bowel (jejunum and ileum) and the colon.

By mimicking the clinical procedure and using an in-house developed software, the GTV was transferred rigidly to each FxsCT by firstly performing a spine match (consisting of a rotation and translation transformations) followed by a fiducial match correction (only translation) [9]. All GTVs transferred to the FxsCT scans were checked by a radiation oncologist by looking at anatomical landmarks such as arteries, veins or other structures. The remaining OAR delineations in the FxsCT were aided by CT-to-CT deformable registration and propagation using commercial software (MIM Software Inc, Cleveland, OH, USA) and edited by the radiation oncologist.

Combining deformable contour registrations

The rigid transformations used for GTV propagation were used to place the FxsCT scans in the pCT coordinate system, i.e. centered at the fiducials center-of-mass. Next, each FxsCT organ triangulated 3D surface mesh was registered non-rigidly to the corresponding pCT organ mesh by using the Thin-Plate Spline Robust-Point Matching (TPS-RPM) algorithm [28], available in our in-house developed software. From each registration, we obtained a Deformation Vector Field (DVF) that provided spatial correspondences between the FxsCT and the pCT organ meshes (Fig. 1A).

Average meshes of the three organs were created by computing the mean DVF in each subject. Subsequently, a second non-rigid registration between the pCT and the FxsCT meshes to the average organs provided all position and shape variations observed in each single patient (Fig. 1B). Quantitative metrics were abstracted per subject: mean surface-to-surface distances (i.e. average length of the DVFs obtained from the non-rigid registrations per patient), volumetric differences, center-of-mass displacements and Dice coefficients (DC). For a dosimetric impact evaluation, differences in V35 (OAR dose-constraint) were acquired on the DVHs, which were computed by taking the original contours and deforming the dose according to the estimated registration between the contours.

A patient with a representative anatomy was selected as reference patient to collect all individuals' variations in a common frame-of-reference (cFOR). Each subject average organ meshes were registered non-rigidly to the average organ meshes of the reference patient (Fig. 1C), whose organ surfaces were discretized with uniformly distributed points at 1.5 mm resolution.

For all the registrations, the parameters of the TPS-RPM were optimized and subsequently evaluated individually for each organ. The transformation accuracy of the registrations was assessed by means of a transformation error (i.e. mean distance between both registered surfaces), and an inverse consistency metric (i.e. mean difference between a forth and back registration between both surfaces) [28,29]. A quality check and visual inspection of the registrations output was also performed. For all the registrations, we achieved an average accuracy and inverse consistency below 1 mm.

Day-to-day OAR motion-deformation model

A population-based motion characterization was performed through a principal component analysis on the propagated organs of all the patients to the cFOR (Fig. 1D). Thus, we tested if abdominal organs move under common patterns, i.e. if OAR change in a correlated way among and within the patients. PCA transforms the original data into a new space of at most N-1 dimensions or modes of variation (being N the total number of observations over all patients, i.e. total number of DVFs). Modes are defined by orthogonal eigenvectors (v) that outline the most dominant

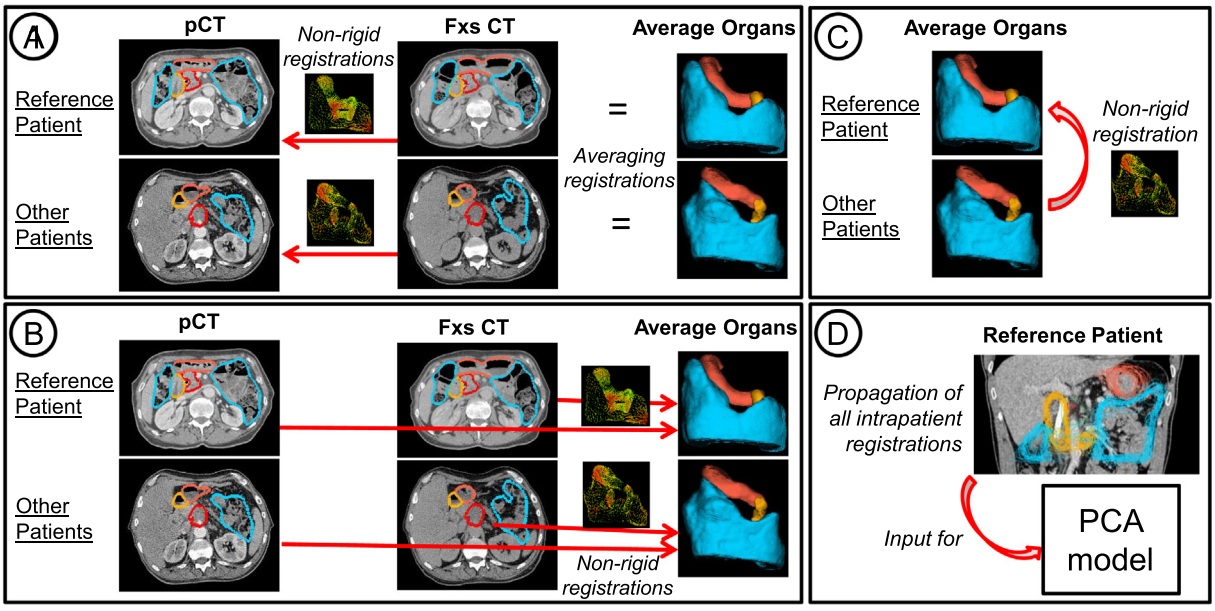

Fig. 1. Workflow used for mapping the intra- and inter-patient anatomical variations onto the reference patient. Firstly (A), daily anatomical variations were registered onto the pCT OAR meshes, and the average OAR was obtained for each patient. Subsequently (B), pCT and daily anatomies were registered onto the average organs. In C, the inter-patient registration among the average organs onto the reference patient allowed the further propagation of all the registrations on the reference patient (D).

directions of daily variations. Each mode is associated to an eigenvalue (λ) that determines its ability to explain the variance in the data. The contribution of each mode in explaining the motion was expressed as the percentage of the sum of the first L eigenvalues from the sum of all eigenvalues [10,11].

A combined gastrointestinal daily motion-deformation statistical model was created from the output of PCA. New deformation vectors fields, leading to new GIO anatomies (GIO_{new}), were created by deforming the mean GI organ (obtained from the average of propagated organs to the cFOR over all patients) by the weighted (b) sum of the first L eigenvectors (Eq. (1)). We compared the performance of two models: including and excluding the bowel.

$$GIO_{new} = GIO_{mean} + \sum_{l=1}^{L} b_l v_l \quad (1)$$

Colormaps were generated to visualize which GIO regions showed the largest motion due to a specific or a set of modes. For this purpose, M (M ~ 5000) points with a Gaussian distribution contained within ±3 standard deviations (SD) were sampled on the first L modes, i.e. random values were given to coefficients b to modulate each eigenvector v_l. A Mersenne Twister Gaussian pseudorandom number generator was used to create the points. Colormaps were built by ranging each mean per-point vector length acquired from the distances between the created organs and the GIO_{mean} shape mesh.

To evaluate whether the population data were representative enough to model GIO daily variations, we applied a leave-one-out-cross-validation approach (LOOCV). Each database subject was pulled out of the training dataset and used as testing patient. Hence, for each case, PCA was calculated on the remaining 34 individuals. The GIO of the left-out-patient (GIO_t) was projected onto the space spanned by the first L eigenvectors to obtain the coefficients (b_t). With the obtained coefficients, GIO_t was reconstructed back using Eq. (1). The PCA model error was computed as the average per-point error vector length acquired from the difference between the original and the reconstructed GIO_t [11,14]. The total model error was averaged from the results on each test patients.

Using the model to create population-based DVHs

As a direct application, the model was used to assess day-to-day OAR motion impact on delivered treatment plans, by also implementing a LOOCV approach. We simulated P (P ~ 5000) random organs with a Gaussian distribution on the first L eigenmodes (within ±3SD), which were propagated back on the average organ of each patient. To ensure the reconstruction of anatomically plausible situations, simulated anatomies overlapping with the GTV were discarded from each simulation. The original dose volume was resampled on the simulated organs to obtain the corresponding DVHs. By selecting the 95% confidence interval range at each bin of the simulated DVHs, we created a population-based DVH for each patient. Retrospectively, we evaluated the DVH widening due to moving-tissues.

Results

Day-to-day OAR motion-deformation within each patient

Volumes of the three critical OAR on the pCT scans were on average (±SD, min–max range): 300 ± 100 ml (100–800 ml) for the stomach; 90 ± 40 ml (40–170 ml) for the duodenum; and 1600 ± 900 ml (200–4700 ml) for the bowel. Volumetric differences between these OAR contoured on the pCT compared to the FxsCTs were on average 100 ± 100 ml, 20 ± 10 ml, and 200 ± 200 ml, respectively (Fig. 2).

Accounting for the study population, non-rigid registrations from the FxsCT to the pCT organ meshes resulted in average mean mesh (per-point) displacements of 10 ± 4 mm (stomach), 6 ± 3 mm (duodenum) and 10 ± 3 mm (bowel) among all FxCT scans. Dice coefficients of mesh overlaps resulted in: 0.80 ± 0.05 (stomach), 0.80 ± 0.08 (duodenum) and 0.80 ± 0.09 (bowel); and center-of-mass displacements in: 11 ± 4 mm (stomach), 8 ± 4 mm (duodenum) and 12 ± 5 mm (bowel).

Propagating the dose from the pCT to the FxsCTs showed an increase of dose-constraint violations (V35Gy > 1 cc) in the FxsCTs with respect to the pCT. In total, 22%, 28% and 11% of all FxsCT

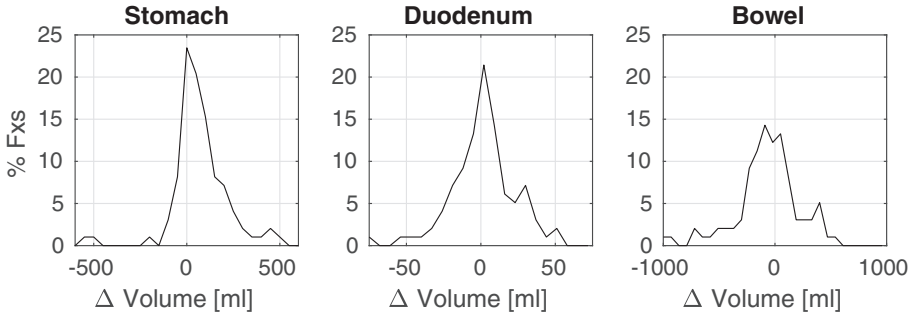

Fig. 2. Histograms of the volumetric differences observed in the stomach, the duodenum and the bowel, acquired by subtracting the FxsCT from the pCT organs.

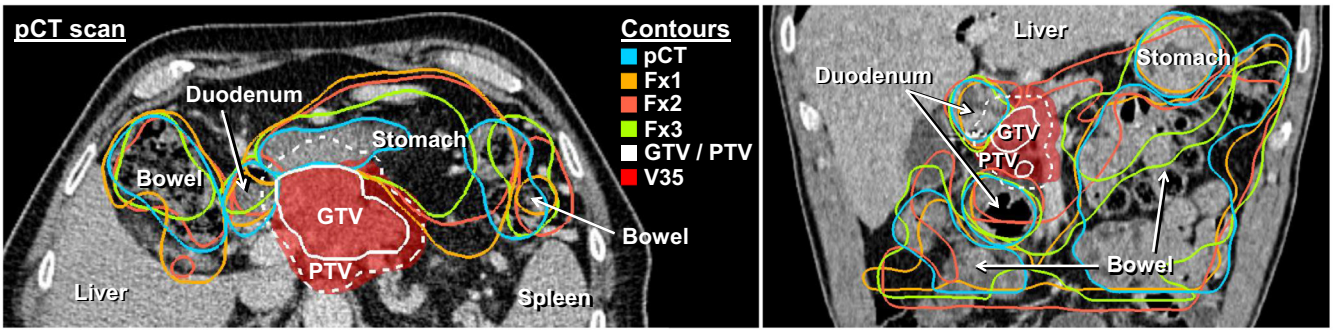

Fig. 3. Depiction of inter-fractional variations of the stomach, duodenum and the bowel after transferring the OAR contours of the FxsCT rigidly onto the pCT scan, on the axial (left) and the coronal (right) views. In red, the V35 isodose line amount overlap with the OAR changes on different days.

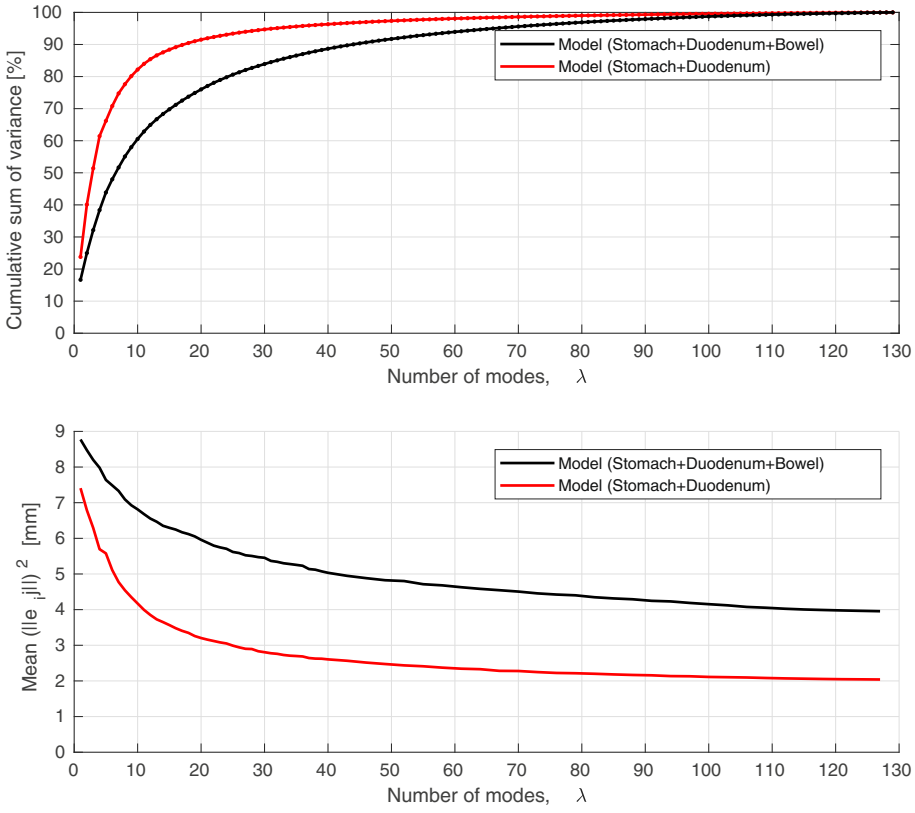

Fig. 4. (Top) Proportion of variance explained by means of the cumulative sum of the eigenvalues associated to each principal component. (Bottom) Mean length of per point error vectors subjected to the number of eigenmodes used during the LOOCV.

scans showed dose-constraint violations for the stomach, the duodenum and the bowel, respectively; whereas in the pCT it was observed to occur in 6%, 11% and 0% of the cases correspondingly. An example of the daily OAR variation effect with respect to the V35 dose-constraint is shown in Fig. 3.

Day-to-day OAR motion-deformation model

Deformations with the largest amplitudes were described by the first eigenmodes. We compared both models including and excluding the bowel. Whereas 19 and 43 modes (out of 130) were required to encapsulate respectively 75% and 90% of the full range of daily motion accounting for the three critical organs, only 7 and 17 modes were needed to explain the most dominant motion-deformation of the stomach and the duodenum (Fig. 4 – top).

When including the bowel in the model, the first three eigenmodes covered 17%, 8% and 7% of the daily variations of the three critical organs. Mode 1 principally describes larger superior-inferior deformations in the upper-lateral regions of the bowel, and an expansion–contraction of the ventral region of the stomach. Mode 2 locates the greatest changes in the top surface of the bowel and in the inferior region of the stomach, which are mainly expanding-contracting in the superior–inferior direction. The duodenum does not significantly vary until mode 3, whose largest changes are in the superior–anterior direction. In further modes, the duodenum mainly varies laterally, but always with lower amplitude (see Fig. 5). Conversely, when excluding the bowel, the first three modes accounted for 24%, 16% and 11% of the variance. In this case, modes 1 and 2 mainly describe displacements toward the anterior-left direction, and the expansion–contraction of the ventral part of the stomach. To a lesser extent, the duodenum displaces laterally in mode 2.

Combining the information above, colormaps quantify the scale of day-to-day motion vectors at each location of the anatomy (Fig. 6). Individual modes deform in particular correlated directions, and therefore, collect motion in specific hotspots. Considering a range of modes, we observe a combined distribution of the daily changes in the anatomy. In the stomach, motion vectors ranged from 5 to 13 mm; in the duodenum, from 4 to 8 mm; and in the bowel, from 7 to 14 mm. Motion was larger in the anterior surfaces, being limited in the inner abdominal cavity closer to the tumor. Modes representing 90% of the variance were comparable to the full motion spectrum. Deformations encapsulated by the residual modes, representing the remaining 10%-variance (43–130th modes for all organs, 17–130th modes for stomach and duodenum) are small, suggesting they describe variations

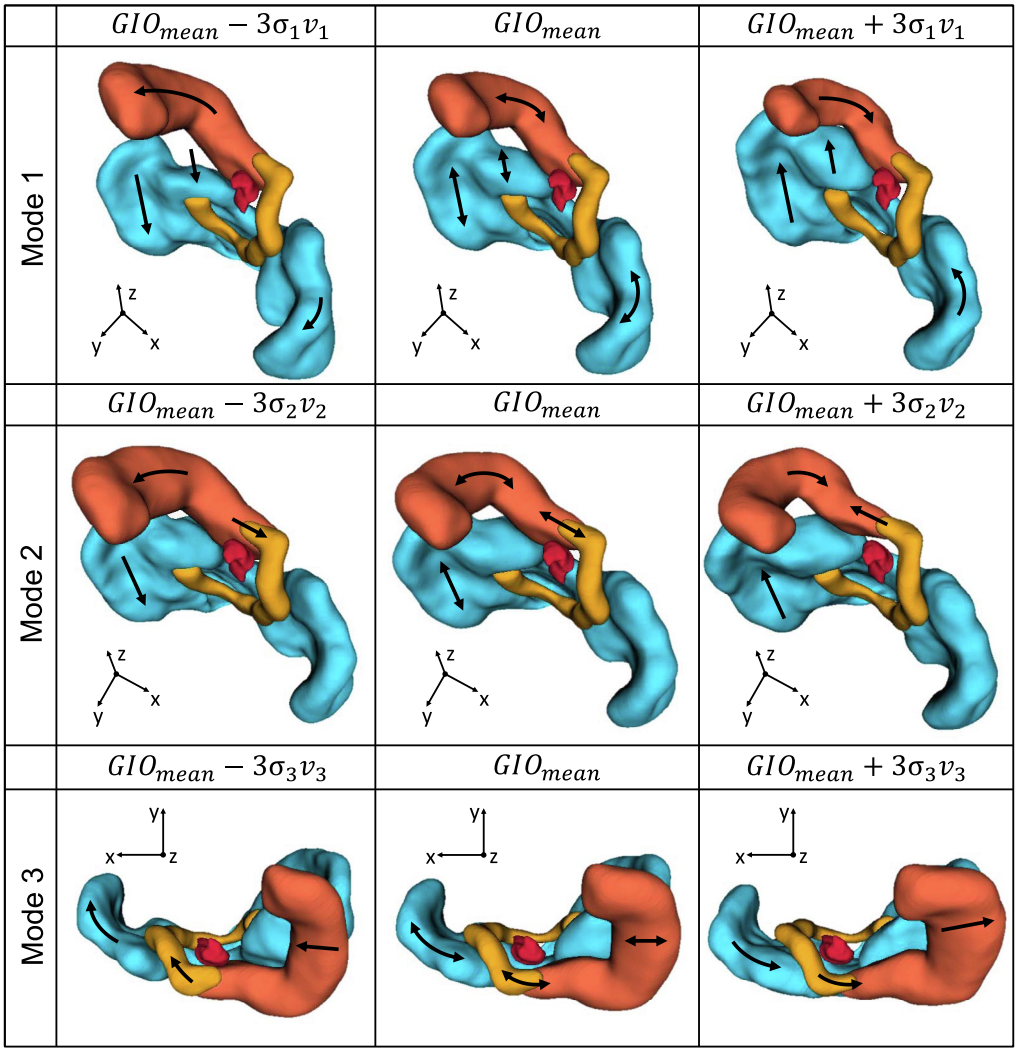

Fig. 5. Depiction of the geometric variations described by the first three modes on the critical organs of the reference patient (in red: tumor; in orange: stomach; in yellow: duodenum; in blue: bowel). The central column shows the direction of motion described individually by each mode on the average population organ (GIO_{mean}). Left and right columns depict the resulting anatomies after deforming the GIO_{mean} organ $\pm 3\sigma_i$ along the respective modes v_i. (For interpretation of the references to color in this figure legend, the reader is referred to the web version of this article.)

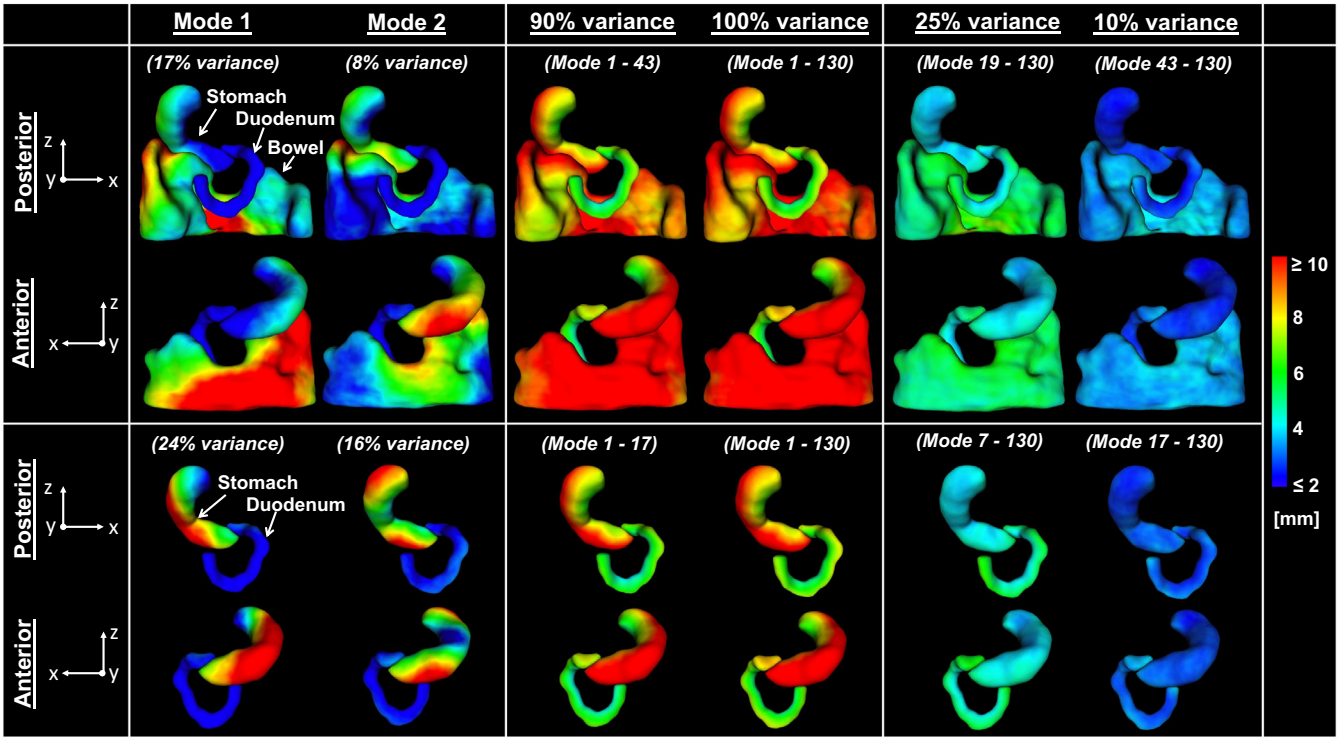

Fig. 6. Anterior and posterior views of the colormaps denoting the motion contained within the first two individual modes of variation against the range of modes contributing to explain the 90%, 100% and residual 25% and 10% of the variance contemplated among our observations. (Top) Model accounting for the three critical organs; (bottom) model accounting only for the stomach and the duodenum. (For interpretation of the references to color in this figure legend, the reader is referred to the web version of this article.)

observed only in few observations within our dataset. Conversely, the residual 25%-variance modes still encapsulate significant deformations as its corresponding colormap depicts mean per-point deformations around 5 mm in each organ.

Model accuracy assessment was performed through the leave-one-out approach. Fig. 4 (bottom) describes the average PCA model error obtained from projecting the left-out-patients onto the space spanned by the first L eigenvectors. As the number of modes L increases, the mean PCA error decreases.

Using the model to create population-based DVHs

Forty-three modes were used to generate population-based DVHs for the three GI organs of each patient. Fig. 7 shows how the tumor position can mitigate or worsen OAR daily motion impact on the simulated DVHs. More than 90% of the clinical DVHs of the whole cohort were contained within the 95% confidence interval of the population-based DVHs, suggesting the model is able to reproduce real anatomies.

Discussion

The observed day-to-day OAR variations in our cohort lead to increased OAR dose-constraint violations when daily organ variations are not considered during SBRT. For this reason, the development of a model that encompasses possible OAR shape and position shifts is of primary interest to improve safety and efficacy during treatment. This is the first study to model daily gastrointestinal organs deformations with respect to the pancreatic tumor position. Large geometrical variations (4–14 mm) have been

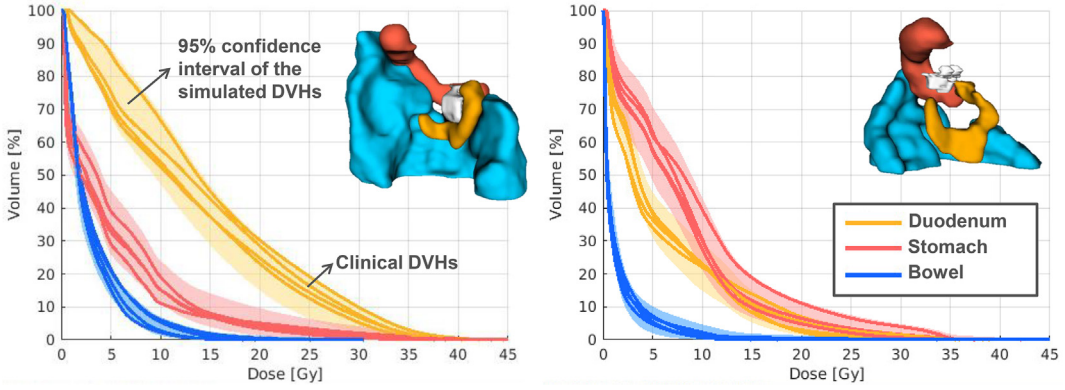

Fig. 7. Depiction of the population-based DVHs simulated for two example patients, obtained by generating OAR motions using the PCA model (including the three OAR: stomach (red), duodenum (orange) and bowel (blue)). In light colors we observe the 95% confidence interval (2.5–97.5% percentile range) of the simulated DVHs, and in solid lines, the real DVHs observed in the clinic for these specific patients. (For interpretation of the references to color in this figure legend, the reader is referred to the web version of this article.)

localized by the first modes of our OAR population-based statistical model, being predominant in the anterior-posterior direction.

The limited number of fractions available per patient did not allow us to model independently the distribution of systematic and random variations. Hence, we restricted ourselves to construct a model that learnt from both types of variations observed in the population. For treatment evaluation purposes, we can use the model to sample the systematic and random component of the anatomies in order to correctly take preparation and execution uncertainties into account.

To our knowledge, only Liu et al. [8] previously attempted to quantify day-to-day anatomical variations on the duodenum and the stomach with respect to the pancreas. Their findings abstracted average center-of-mass displacements of 6 and 10 mm respectively, and Dice coefficients of 0.7 (for both organs). Accounting for delineation errors (of <2 mm) in both studies, their results agree well with our intra-patient analysis, where average center-of-mass displacements of 8 mm (duodenum) and 11 mm (stomach), and DC of 0.8 were observed.

In our case, geometrical variations were quantified based on the estimated TPS-RPM transformations. This method is based on the registration of points on the 3D surface meshes, and inner points can be estimated from the interpolation of the obtained transformation. Nonetheless, we do not expect this significantly impacts our results, since our OAR are hollow and we were mainly interested in the position of the organ walls.

Clearly, these geometrical variations have dosimetric consequences: the increase of dose-constraint violations (V35 > 1 ml) in our cohort suggests that daily organ deformations are likely to result in parts of organs entering the V35 region, due to their proximity to the tumor and the strongly sculpted doses in the pCT.

Learning to simulate realistic geometries through our model can aid to interpret these dosimetric uncertainties [18]. For this purpose, the model was firstly used to separate the modes describing correlated daily motion from uncorrelated movement and noise. Subsequently, we judged its quality based on the number of modes used. Other authors [10,11,18,23] tried to find a balance between the ability of the modes in explaining the variability of the samples and their capacity to accurately predict unknown anatomies. In our case, both criteria were highly influenced by the inclusion of the bowel into the model. Bowels are large, complex and highly variable structures among our patients; and despite trying to keep delineation consistency, bowels could significantly differ in terms of the information they represent in each subject. For this reason, we assessed the performance of the model including and excluding this organ. When including it, this organ variability could explain why the accuracy error obtained during the prediction of unknown anatomies through the LOOCV increases a factor of 2, suggesting that some small patient-specific deformations might not be captured. On the contrary, if excluding it, less variability of the data needs to be analyzed, and hence, fewer modes are required to achieve better modeling accuracy. In comparison, only 17 modes instead of 43 would already represent 90% of the variance in the second case. Thus, the bowel can be modeled, but at the expense of increasing the model complexity.

Compared with other models in the literature, gastrointestinal organs variations seem to be more difficult to capture by the first modes, suggesting that their deformations are less generic than in other treatment sides. Whereas our first mode covered 17% or 24% of the variations (when including and excluding the bowel); in a bladder-prostate model, the first mode could already capture up to 40–60% of variability [15,18] (corresponding to bladder filling); and in a prostate-seminal vesicles model [11] or a rectum model [17], the first mode could cover 35% and 30%, respectively.

Through the colormaps we assessed the impact of selecting ranges of modes. Capturing 90% of the variance appears to be representative enough to locate realistic average daily variations on the abdominal anatomy (10 mm on the stomach and bowel, and 6 mm on the duodenum), as exactly observed in our intra-patient analysis. Hence, modes representing 90% of the variance already encapsulate the strongest common patterns observed in the data. The remaining 10%-variance mode range does not represent large deformations on the organs in any case. Therefore, we can decide to not consider them in our simulations.

Because of the abovementioned observations, to test daily motion impact on clinical plans for the three critical organs, we finally used 43 modes to perform patient-specific population-based DVHs. Through the LOOCV, we evaluated if we could generate alternative anatomies resembling real organs for an "unknown" patient. By sampling daily OAR motion from the statistical model, clinical DVHs fell within the simulated DVH ranges in most of the cases (>90%).

In summary, we have shown that relative day-to-day motion of the gastrointestinal organs with respect to pancreatic tumors can significantly influence the delivered doses to the organs-at-risk. PCA has been used to find variation patterns in our cohort, and to generate meaningful anatomies reproducing clinically delivered doses. OAR motion simulations can be further explored to correlate the dosimetric impact of OAR motion to reported toxicities, to investigate meaningful anatomies for a Plan-of-the-Day strategy, or to be used in automatic plan optimization.

Conflicts of interest

This work was in part funded by a research grant of Accuray Inc., Sunnyvale, USA. Erasmus MC Cancer Institute also has a research collaboration with Elekta AB, Stockholm, Sweden.

Acknowledgement

The authors wish to thank Warren Kilby from Accuray research and development team, for providing valuable insight and carefully reviewing this manuscript.

References

[1] Buwenge M, Cellini F, Silvestris N, Cilla S, Deodato F, Macchia G, et al. Robotic radiosurgery in pancreatic cancer: a systematic review. World J Gastroenterol 2015;21:9420–9. https://doi.org/10.3748/wjg.v21.i31.9420.

[2] Chuong MD, Springett GM, Freilich JM, Park CK, Weber JM, Mellon EA, et al. Stereotactic body radiation therapy for locally advanced and borderline resectable pancreatic cancer is effective and well tolerated. Int J Radiat Oncol Biol Phys 2013;86:516–22. https://doi.org/10.1016/j.ijrobp.2013.02.022.

[3] Goyal K, Einstein D, Ibarra R, Yao M, Kunos C, Ellis R, et al. Stereotactic body radiation therapy for non-resectable tumors of the pancreas. J Surg Res 2012;174:319–25. https://doi.org/10.1080/10810730902873927.Testing.

[4] Petrelli F, Comito T, Ghidini A, Torri V, Scorsetti M, Barni S. Stereotactic body radiation therapy for locally advanced pancreatic cancer: a systematic review and pooled analysis of 19 trials. Int J Radiat Oncol 2017;97:313–22. https://doi.org/10.1016/j.ijrobp.2016.10.030.

[5] Loi M, Magallon-Baro A, Papalazarou C, Milder M, Nuyttens JJ. Robotic stereotactic treatment for malignant metastasis of solid tumour in the pancreas: a multiple case report and review of literature. Cancer Radiother 2017;21:784–7. https://doi.org/10.1016/j.canrad.2017.06.012.

[6] Hoogeman M, Prévost J-B, Nuyttens J, Pöll J, Levendag P, Heijmen B. Clinical accuracy of the respiratory tumor tracking system of the CyberKnife: assessment by analysis of log files. Int J Radiat Oncol Biol Phys 2009;74:297–303. https://doi.org/10.1016/J.IJROBP.2008.12.041.

[7] Kilby W, Dooley JR, Kuduvalli G, Sayeh S, Maurer CR. The CyberKnife® robotic radiosurgery system in. Technol Cancer Res Treat 2010;2010:433–52. https://doi.org/10.1177/153303461000900502.

[8] Liu F, Erickson BA, Peng C, Li XA. Characterization and management of interfractional anatomic changes for pancreatic cancer radiotherapy. Int J Radiat Oncol Biol Phys 2012;83:423–9. https://doi.org/10.1016/j.ijrobp.2011.12.073.

[9] Papalazarou C, Klop GJ, Milder MTW, Marijnissen JPA, Gupta V, Heijmen BJM, et al. CyberKnife with integrated CT-on-rails: System description and first clinical application for pancreas SBRT. Med Phys 2017;44:4816–27. https://doi.org/10.1002/mp.12432.

[10] Söhn M, Birkner M, Yan D, Alber M. Modelling individual geometric variation based on dominant eigenmodes of organ deformation: Implementation and evaluation. Phys Med Biol 2005;50:5893–908. https://doi.org/10.1088/0031-9155/50/24/009.
[11] Budiarto E, Keijzer M, Storchi PR, Hoogeman MS, Bondar L, Mutanga TF, et al. A population-based model to describe geometrical uncertainties in radiotherapy: applied to prostate cases. Phys Med Biol 2011;56:1045–61. https://doi.org/10.1088/0031-9155/56/4/011.
[12] Thörnqvist S, Hysing LB, Zolnay AG, Söhn M, Hoogeman MS, Muren LP, et al. Adaptive radiotherapy in locally advanced prostate cancer using a statistical deformable motion model. Acta Oncol (Madr) 2013;52:1423–9. https://doi.org/10.3109/0284186X.2013.818249.
[13] Hu Y, Gibson E, Ahmed HU, Moore CM, Emberton M, Barratt DC. Population-based prediction of subject-specific prostate deformation for MR-to-ultrasound image registration. Med Image Anal 2015;26:332–44. https://doi.org/10.1016/j.media.2015.10.006.
[14] Szeto YZ, Witte MG, van Herk M, Sonke JJ. A population based statistical model for daily geometric variations in the thorax. Radiother Oncol 2017;123:99–105. https://doi.org/10.1016/j.radonc.2017.02.012.
[15] Rios R, De Crevoisier R, Ospina JD, Commandeur F, Lafond C, Simon A, et al. Population model of bladder motion and deformation based on dominant eigenmodes and mixed-effects models in prostate cancer radiotherapy. Med Image Anal 2017;38:133–49. https://doi.org/10.1016/j.media.2017.03.001.
[16] Thörnqvist S, Hysing LB, Zolnay AG, Söhn M, Hoogeman MS, Muren LP, et al. Treatment simulations with a statistical deformable motion model to evaluate margins for multiple targets in radiotherapy for high-risk prostate cancer. Radiother Oncol 2013;109:344–9. https://doi.org/10.1016/j.radonc.2013.09.012.
[17] Bondar L, Intven M, Burbach JPM, Budiarto E, Kleijnen JP, Philippens M, et al. Statistical modeling of CTV motion and deformation for IMRT of early-stage rectal cancer. Int J Radiat Oncol Biol Phys 2014;90:664–72. https://doi.org/10.1016/j.ijrobp.2014.06.040.
[18] Söhn M, Sobotta B, Alber M. Dosimetric treatment course simulation based on a statistical model of deformable organ motion. Phys Med Biol 2012;57:3693–709. https://doi.org/10.1088/0031-9155/57/12/3693.
[19] Nie X, Liang J, Yan D. Organ sample generator for expected treatment dose construction and adaptive inverse planning optimization. Med Phys 2012;39:7329–37. https://doi.org/10.1118/1.4765457.
[20] Xu H, Vile DJ, Sharma M, Gordon JJ, Siebers JV. Coverage-based treatment planning to accommodate deformable organ variations in prostate cancer treatment. Med Phys 2014;41:. https://doi.org/10.1118/1.4894701101705.
[21] Cai W, Hurwitz MH, Williams CL, Dhou S, Berbeco RI, Seco J, et al. 3D delivered dose assessment using a 4DCT-based motion model. Med Phys 2015;42:2897–907. https://doi.org/10.1118/1.4921041.
[22] Zhang Q, Pevsner A, Hertanto A, Hu YC, Rosenzweig KE, Ling CC, et al. A patient-specific respiratory model of anatomical motion for radiation treatment planning. Med Phys 2007;34:4772–81. https://doi.org/10.1118/1.2804576.
[23] Badawi AM, Weiss E, Sleeman WC, Yan C, Hugo GD. Optimizing principal component models for representing interfraction variation in lung cancer radiotherapy. Med Phys 2010;37:5080–91. https://doi.org/10.1118/1.3481506.
[24] Li R, Lewis JH, Jia X, Zhao T, Liu W, Wuenschel S, et al. On a PCA-based lung motion model. Phys Med Biol 2011;56:6009–30. https://doi.org/10.1088/0031-9155/56/18/015.
[25] Stemkens B, Tijssen RHN, De Senneville BD, Lagendijk JJW, Van Den Berg CAT. Image-driven, model-based 3D abdominal motion estimation for MR-guided radiotherapy. Phys Med Biol 2016;61:5335–55. https://doi.org/10.1088/0031-9155/61/14/5335.
[26] Kontaxis C, Bol GH, Stemkens B, Glitzner M, Prins FM, Kerkmeijer LGW, et al. Towards fast online intrafraction replanning for free-breathing stereotactic body radiation therapy with the MR-linac. Phys Med Biol 2017;62:7233–48. https://doi.org/10.1088/1361-6560/aa82ae.
[27] Jabbour SK, Hashem SA, Bosch W, Kim TK, Finkelstein SE, Anderson BM, et al. Upper abdominal normal organ contouring guidelines and atlas: a radiation therapy oncology group consensus. Pract Radiat Oncol 2014;4:82–9. https://doi.org/10.1016/j.prro.2013.06.004.
[28] Vásquez Osorio EM, Hoogeman MS, Bondar L, Levendag PC, Heijmen BJM. A novel flexible framework with automatic feature correspondence optimization for nonrigid registration in radiotherapy. Med Phys 2009;36:2848–59. https://doi.org/10.1118/1.3134242.
[29] Bondar L, Hoogeman MS, Vásquez Osorio EM, Heijmen BJM. A symmetric nonrigid registration method to handle large organ deformations in cervical cancer patients. Med Phys 2010;37:3760–72. https://doi.org/10.1118/1.3443436.